

## Apparatus for deposition of composition spread alloy films: The rotatable shadow mask

Benoit Fleutot, James B. Miller, and Andrew J. Gellman

Citation: *Journal of Vacuum Science & Technology A* **30**, 061511 (2012); doi: 10.1116/1.4766194

View online: <http://dx.doi.org/10.1116/1.4766194>

View Table of Contents: <http://scitation.aip.org/content/avs/journal/jvsta/30/6?ver=pdfcov>

Published by the AVS: Science & Technology of Materials, Interfaces, and Processing

### Articles you may be interested in

[Compact tool for deposition of composition spread alloy films](#)

*J. Vac. Sci. Technol. A* **30**, 011503 (2012); 10.1116/1.3664078

[Improved GaN film overgrown with a molybdenum nanoisland mask](#)

*Appl. Phys. Lett.* **93**, 031906 (2008); 10.1063/1.2962983

[Spreading of thin-film metal patterns deposited on nonplanar surfaces using a shadow mask micromachined in Si \(110\)](#)

*J. Vac. Sci. Technol. B* **25**, 1207 (2007); 10.1116/1.2747629

[Preparation of ternary alloy libraries for high-throughput screening of material properties by means of thick film deposition and interdiffusion: Benefits and limitations](#)

*J. Vac. Sci. Technol. A* **22**, 1788 (2004); 10.1116/1.1692366

[Resistless pattern definition and Si selective-area deposition using an ultrathin SiO<sub>2</sub> mask layer treated by SiHCl<sub>3</sub>](#)

*Appl. Phys. Lett.* **76**, 3203 (2000); 10.1063/1.126629



## Instruments for Advanced Science

<p>Contact Hiden Analytical for further details:  <b>W</b> <a href="http://www.HidenAnalytical.com">www.HidenAnalytical.com</a>  <b>E</b> <a href="mailto:info@hiden.co.uk">info@hiden.co.uk</a></p> <p><a href="#">CLICK TO VIEW</a> our product catalogue</p>	 <p><b>Gas Analysis</b></p> <ul style="list-style-type: none"> <li>› dynamic measurement of reaction gas streams</li> <li>› catalysis and thermal analysis</li> <li>› molecular beam studies</li> <li>› dissolved species probes</li> <li>› fermentation, environmental and ecological studies</li> </ul>	 <p><b>Surface Science</b></p> <ul style="list-style-type: none"> <li>› UHV TPD</li> <li>› SIMS</li> <li>› end point detection in ion beam etch</li> <li>› elemental imaging - surface mapping</li> </ul>	 <p><b>Plasma Diagnostics</b></p> <ul style="list-style-type: none"> <li>› plasma source characterization</li> <li>› etch and deposition process reaction</li> <li>› kinetic studies</li> <li>› analysis of neutral and radical species</li> </ul>	 <p><b>Vacuum Analysis</b></p> <ul style="list-style-type: none"> <li>› partial pressure measurement and control of process gases</li> <li>› reactive sputter process control</li> <li>› vacuum diagnostics</li> <li>› vacuum coating process monitoring</li> </ul>
---	--	--	--	--

# Apparatus for deposition of composition spread alloy films: The rotatable shadow mask

Benoit Fleutot

*Department of Chemical Engineering, Carnegie Mellon University, Pittsburgh, Pennsylvania 15213*

James B. Miller and Andrew J. Gellman<sup>a)</sup>

*National Energy Technology Laboratory-Regional University Alliance (NETL-RUA), US Department of Energy, Pittsburgh, Pennsylvania 15236 and Department of Chemical Engineering, Carnegie Mellon University, Pittsburgh, Pennsylvania 15213*

(Received 17 July 2012; accepted 18 October 2012; published 9 November 2012)

Composition spread alloy films (CSAFs) are materials libraries used for high throughput investigations of multicomponent materials such as alloys,  $A_xB_yC_{1-x-y}$ . CSAFs are prepared such that the alloy film has a lateral spatial gradient in its local composition; thus, they include a set of alloy samples with a distribution of compositions that spans a continuous region of composition space  $(x,y)$ . A tool based on the shadow mask concept has been developed for generating composition gradients, but modified to allow rotation of the shadow mask during CSAF deposition. The tool allows deposition of CSAFs containing up to four elements with rotatable shadow masks between each of the four electron beam evaporation sources and the deposition substrate. This allows codeposition of any combination of up to four components. In the case of the ternary  $A_xB_yC_{1-x-y}$  CSAFs, the three components can be deposited such that the resulting CSAF spans the entire ternary alloy composition space ( $x=0 \rightarrow 1$ ,  $y=0 \rightarrow 1-x$ ) and, furthermore, contains all three binary alloys  $A_xB_{1-x}$ ,  $A_xC_{1-x}$ , and  $B_xC_{1-x}$  ( $x=0 \rightarrow 1$ ) and all three pure components. The innovation of the rotatable shadow masks also allows preparation of CSAFs that magnify selected regions of the composition space ( $x=x_{\min} \rightarrow x_{\max}$ ,  $y=y_{\min} \rightarrow 1-x$ ). Herein, we describe the design and performance of this new CSAF deposition tool and assess its merits and limitations with respect to other methods for CSAF preparation. © 2012 American Vacuum Society. [http://dx.doi.org/10.1116/1.4766194]

## I. INTRODUCTION

Multicomponent materials such as alloys,  $A_xB_{1-x}$  and  $A_xB_yC_{1-x-y}$ , typically have useful properties that are superior to those of their pure components. However, the challenge in multicomponent materials development is that the exhaustive search of composition space to find the optimal composition for a given application can be experimentally daunting. The problem is that it requires the fabrication, characterization, and study of large numbers of samples. Furthermore, a key barrier to understanding the properties of multicomponent alloys and developing them for specific applications is that many of their important properties are continuous functions of alloy composition  $(x, y)$ . The composition dependence of alloy properties cannot be completely understood based solely on studies of a few single-composition samples. Understanding the characteristics and properties of multicomponent materials requires measurement and modeling methods that can span composition space.

Over the past decade, high throughput approaches for preparation and characterization of multicomponent materials have been developed to accelerate both materials science and the process of materials discovery and optimization.<sup>1,2</sup> These high throughput methods have been popularized in the biomolecular sciences, catalysis, electrochemistry, photovol-

taic sciences, and other areas of materials science.<sup>3-12</sup> High throughput methods have three principal elements. The first is the preparation of large numbers of different materials samples that form the elements of a materials library. The second is the rapid, high throughput characterization of these materials to determine the composition, structure, phase distribution, etc. across the entire library. And the third is the ability to make high throughput measurements across the library of the materials properties relevant to the specific application of interest: catalytic activity, hardness, thermal conductivity, etc. The combined suite of capabilities can accelerate the study and development of multicomponent materials by orders of magnitude.

Many high throughput investigations of multicomponent materials use libraries based on composition spread alloy films (CSAFs), which are thin alloy films deposited in such a way that there is a lateral gradient in their local composition (Fig. 1).<sup>9,13,14</sup> CSAFs are materials libraries that contain continuous composition distributions of binary or higher-order alloys on a single compact substrate. These can span entire composition spaces or focus on composition subspaces of interest. When spatially resolved methods are used to characterize their composition and functional properties, CSAF libraries allow rapid determination of composition-property relationships across broad, continuous regions of alloy composition space.

In this paper, we describe the design, operation, and performance of a new CSAF deposition tool based on the concept of a rotatable shadow mask and capable of depositing

<sup>a)</sup> Author to whom correspondence should be addressed; electronic mail: gellman@cmu.edu

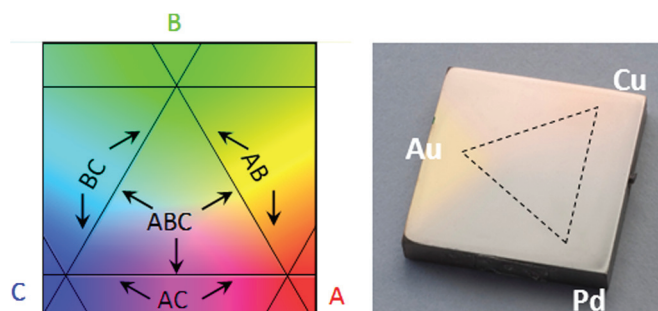


Fig. 1. (Color) Left: Schematic representation of a CSAF generated by the RSM-CSAF deposition tool with regions containing the entire ternary alloy composition space,  $A_xB_yC_{1-x-y}$  ( $x=0 \rightarrow 1$ ,  $y=0 \rightarrow 1-x$ ), all three binary alloys  $A_xB_{1-x}$ ,  $A_xC_{1-x}$ , and  $B_xC_{1-x}$  ( $x=0 \rightarrow 1$ ) and all three pure components. Right: Photograph of a Cu<sub>x</sub>Au<sub>y</sub>Pd<sub>1-x-y</sub> CSAF. In color, the Au, Cu, and Pd regions are readily identifiable.

CSAFs of up to four elemental components. Herein, we refer to this tool as the rotating shadow mask CSAF (RSM-CSAF) deposition tool. The individual components can be deposited simultaneously from electron beam physical vapor deposition sources, thus allowing preparation of CSAFs that can contain most metallic elements of the periodic table. Multicomponent materials with lateral composition gradients are deposited in such a way that both the direction and the amplitude of the composition gradient can be controlled independently for all four components. The UHV chamber housing the RSM-CSAF deposition tool can be interfaced with other UHV apparatus containing the tools for bulk and surface characterization necessary to establish the structure–composition–property relationships of a multicomponent alloy.

## II. METHODS FOR PREPARATION OF CSAFs

Before describing the RSM-CSAF deposition technique, we review briefly other CSAF preparation methods. The use of CSAFs has a long history beginning in the 1950s and motivated by interest in the determination of alloy phase diagrams.<sup>13,15</sup> Although the CSAF concept as a library or platform for accelerated study of multicomponent materials has existed for decades, early implementations were limited in scope and impact. To a large extent, their use was limited by the availability of the complementary data acquisition and analysis tools needed for high throughput characterization. Key developments of the past decade have been increased availability of spatially resolving characterization tools and the computational tools for automated data acquisition and analysis.<sup>13,15–18</sup>

Various metrics can be used to compare the merits of different CSAF deposition methods. One category of metrics describes the quality of the final CSAF. For example, one can consider the achievable composition span in the range  $x=0 \rightarrow 1$  for each component and the ability to control that composition span. Related to this is the purity of the film, or in other words, the minimization of contaminants. Another metric is the degree of component intermixing and thus the ability to generate the thermodynamically stable phases

associated with the local composition. A second category of metrics for comparison of different CSAF deposition methods are related to the method itself. This includes the breadth of different elements that can be deposited by the given method and the number of elemental components that can be included in a single CSAF. Related metrics include the range of attainable CSAF thicknesses and the growth rates. For many studies, the physical size of the composition spread may be an issue. A third category of metrics includes issues of practicality and utility such as cost of the instrumentation, complexity, and throughput. Needless to say, no single method for CSAF preparation scores perfectly across all metrics.

One approach, as shown in Fig. 2(a), uses chemical vapor deposition (CVD) to produce composition spreads by positioning the CVD precursor inlets close to the substrate and allowing diffusive, gas phase intermixing to create the composition gradient on the substrate in the region between the two sources.<sup>19,20</sup> The local film growth rate is dependent on the precursors, their flux to the substrate surface and the substrate temperature. This method is relatively simple and does allow codeposition of components for intimate mixing. However, it allows limited control of the composition span for a given film and generates films of nonuniform thickness.

A second approach, presented in Fig. 2(b), uses sources that give a uniform flux to the substrate and a contact mask, which slides across the substrate surface to vary the effective deposition time, and thus, the thickness at different locations on the substrate.<sup>21–23</sup> The CSAFs are generated by sequential deposition of components with gradients in different directions. One of the limitations of this method is that the components cannot be codeposited and subsequent annealing may not lead to complete mixing, unless each layer is no more than one atomic monolayer in thickness. On the other

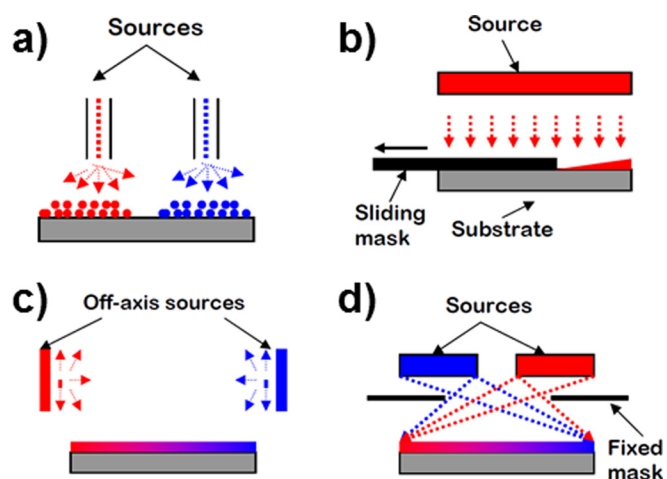


Fig. 2. (Color online) Schematic representations of four methods for generating composition spread alloy films. (a) Chemical vapor deposition sources positioned close to the substrate such that lateral diffusion in the gas phase results in a gradient in flux to the surface from each source. (b) Deposition of individual components in wedges using a sliding contact mask. (c) Offset positioning of sources to generate nonuniform flux distributions across the substrate surface. (d) Simultaneous deposition of multiple components using fixed shadow masks to form the composition gradients.

hand, it does allow a very high degree of control over the direction and the span of the composition gradient. It also allows the composition to have arbitrary (but monotonic) variation across the substrate.

Another method for forming CSAFs is to use off-axis sources [Fig. 2(c)]. In this method, sources are positioned off-axis relative to the substrate surface.<sup>13,24</sup> This results in gradients in their flux across the substrate. CSAFs are formed by intermixing of fluxes from multiple sources. A simple, compact offset filament deposition tool with up to four sources has been developed in our laboratory.<sup>25</sup> In its current design, the tool is capable of repeatable, quantitative production of thin ( $\leq 100$  nm) CSAFs on substrates that are up to  $\sim 12$  mm across. The system can be used to deposit any metal or other material that is evaporable at temperatures up to  $\sim 1500$  K. It can produce fluxes that vary by over an order of magnitude across the substrate surface. This design has a number of merits but some limitations in functionality. One benefit over the masking method is that it has no moving parts. In general, the offset source methods have the benefit of allowing codeposition of several components, but they do not allow the full span of composition space to be accessed on a single CSAF. Figure 3 illustrates the composition spread of a typical CSAF deposited using our offset filament deposition tool.<sup>25</sup> Although the region spanned by a single CSAF can be controlled by controlling the source fluxes, no single CSAF generated by the offset source method can span the entire ternary composition space.

The shadow mask method [Fig. 2(d)] uses multiple sources operating simultaneously with shadow masks positioned between the sources and the substrate.<sup>26,27</sup> Because the source has finite width and the shadow is positioned between the source and the substrate, different points on the substrate are shadowed from varying portions of the source. The pen-

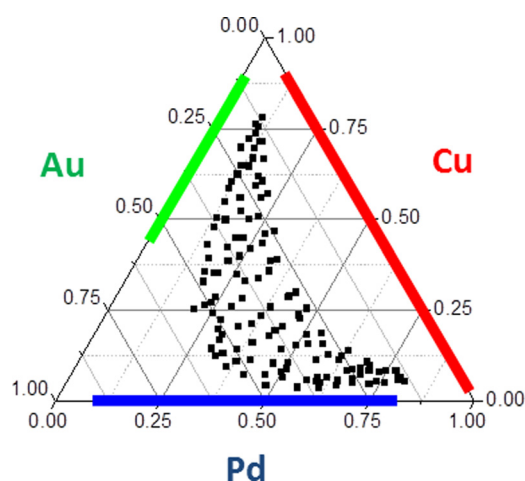


FIG. 3. (Color online) Illustration of the region of a ternary alloy composition space spanned by a CSAF generated using an offset filament CSAF deposition tool (Ref. 25). The bars on the edges of the ternary composition diagram illustrate the composition ranges of each of the three components. This limited coverage of composition space is typical of CSAF deposition methods that do not have some means of reducing the flux of each component to zero at some point across the CSAF.

umbra of the shadow creates a linear gradient in flux varying from a maximum at points exposed to the entire source to zero at points completely shadowed from the source. With no moving parts, this technique allows simultaneous deposition of multiple components across the substrate with linear gradients in composition along directions dictated by the positioning of the masks. The shadow mask CSAF deposition method allows codeposition of components with flux gradients that generate CSAFs that span the entire composition space. The shadow mask method itself is described thoroughly in Refs. 26 and 27 and allows fairly easy quantification of the relationship between the local flux across the substrate and the geometric parameters describing the sizes and the relative positions of the source, substrate, and mask. Herein, we describe a specific implementation of the shadow mask method that incorporates four e-beam sources onto a compact 254 mm CF flange and uses rotatable shadow masks to allow arbitrary orientation of the composition gradient from each source and to control the magnitude of the gradient to cover any fraction of the range from 0 to 100% of full flux from any given source.

#### A. Rotatable shadow mask CSAF deposition tool

The positioning of the shadow mask between the source and the substrate determines the location and the spatial extent of the flux gradient at the substrate surface [Fig. 2(d)]. If one thinks of the shadow mask concept in 3D, as illustrated in Fig. 4, it is obvious that the orientation of the shadow mask can also be used to control the direction of the flux gradient across the substrate. Furthermore, if the shadow mask can be rotated during deposition, one can control the net flux at either end of the gradient spread. These possibilities have motivated our design and fabrication of the RSM-CSAF deposition tool.

One of the attractive features of the rotating shadow mask concept is that with three active sources, one can orient the flux gradients at  $120^\circ$  from one another to create a composition distribution resembling a triangular ternary composition diagram. In fact, the flux field can be established such that it

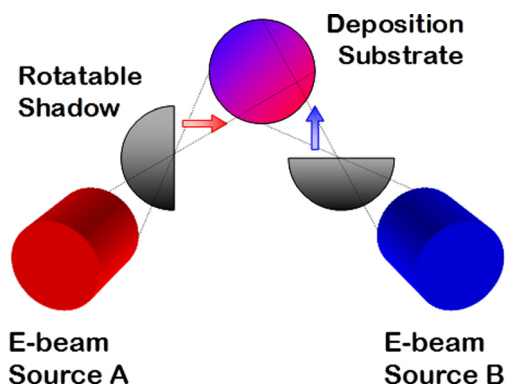


FIG. 4. (Color online) Conceptual schematic of the rotating shadow mask CSAF deposition tool. The sources are “flat” in that they emit their materials across a finite area rather than being point sources. The orientation of the shadow masks dictates the orientation of the composition gradient from each source.

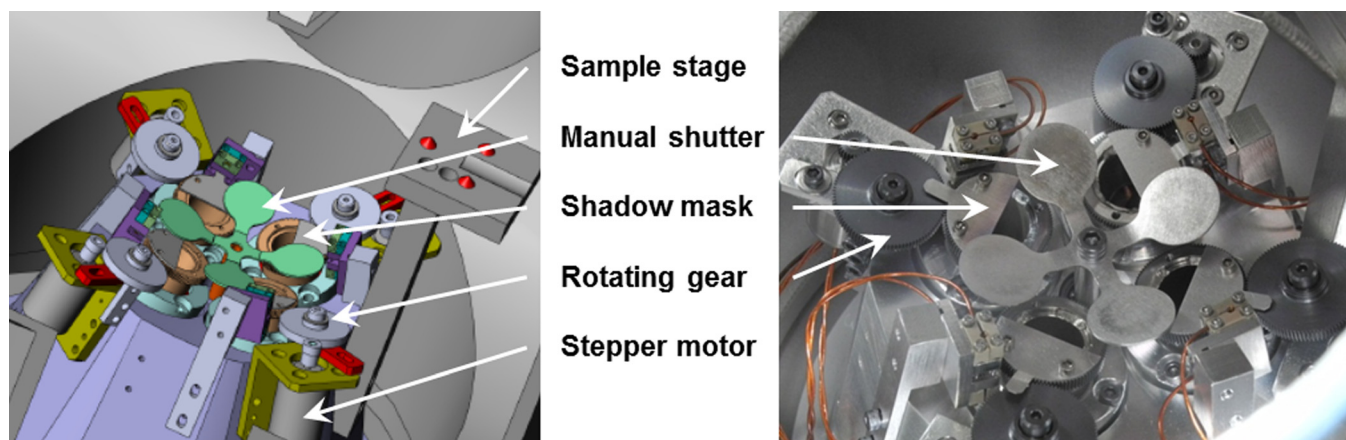


FIG. 5. (Color online) (a) 3D rendering of the RSM-CSAF deposition tool. (b) Picture of the deposition tool inside the ultrahigh vacuum chamber.

produces the CSAF illustrated in Fig. 1. In the middle is the triangular region that spans all of ternary alloy composition space,  $A_xB_yC_{1-x-y}$  with  $x=0 \rightarrow 1$  and  $y=0 \rightarrow 1-x$ . The regions outside the edges of the ternary triangle contain all three binary composition spreads,  $A_xB_{1-x}$ ,  $A_xC_{1-x}$ , and  $B_xC_{1-x}$  with  $x=0 \rightarrow 1$ . Outside the vertices of the ternary triangle are regions (not points) that contain only the pure components, A, B, or C. Having regions that contain the pure components becomes extremely useful for calibration of the analytical tools that are used to characterize the CSAF. Equally importantly, the fact that the shadow masks can be rotated during deposition means that the composition range spanned by the ternary triangle can be controlled to span any subspace of the ternary composition space,  $A_xB_yC_{1-x-y}$  with  $x=x_{\min} \rightarrow x_{\max}$  and  $y=y_{\min} \rightarrow (1-x)$ . This effectively magnifies the selected region of composition space to occupy the full triangular region in the middle of the CSAF. Unlike the approach described in earlier work, this can be done without changing the source fluxes.<sup>26,27</sup> In other words, with all three source fluxes being equal, one can prepare a CSAF with the full ternary composition spread (Fig. 1) or any triangular subspace of the ternary composition space, simply by controlled rotation of the shadow mask.

One of the valuable features of our design for the RSM-CSAF deposition tool is that it is relatively compact compared to previous implementations.<sup>26,27</sup> Our RSM-CSAF deposition tool is entirely mounted on a standard 254 mm Conflat™ flange (CF) used in a UHV chamber. As a result, it can be mounted and dismounted from a UHV chamber fairly easily for maintenance. The tool is illustrated and photographed in Fig. 5. It has four electron beam evaporation sources on 70 mm CFs recessed in tubes that are angled at  $15^\circ$  from the normal of the 254 mm CF and aimed at a point that is 190 mm from the flange face along its center line. During deposition, the substrate is positioned at this focal point. The substrate is shadowed from the four sources by four independently rotatable, semicircular masks that are rotated by geared UHV stepper motors. The stepper motors can rotate the shadow masks independently and under com-

puter control. Figure 6 shows a cross section through the RSM-CSAF deposition tool. The critical dimensions of the RSM-CSAF tool are that the e-beam sources have source diameters of 5 mm; the distance from the sources to the substrate is 135 mm, and the rotating shadow mask is positioned 45 mm from the source. This design should result in a linear flux gradient across a 10 mm region of the substrate. Provided that the sources are aligned such that the spatial extent of the gradient lies within the dimensions of the substrate and that the shadow masks are oriented at  $120^\circ$  from one another, a CSAF of the type illustrated in Fig. 1 will be deposited on the substrate.

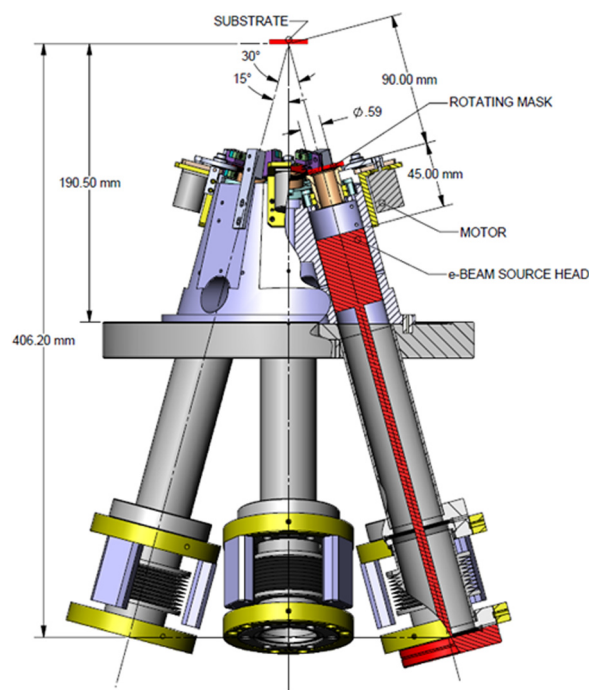


FIG. 6. (Color online) Schematic cross section through the RSM-CSAF deposition tool. The sources are angled at  $15^\circ$  with respect to the substrate normal. The shadow masks are located at one third of the distance from the source to the substrate. The source diameter is 5 mm, and the nominal gradient width on the substrate is 10 mm.

The CSAF substrates are  $12 \times 12 \text{ mm}^2$  of 2 mm thick Mo. Mo has been chosen for most substrates because very few metals will alloy with Mo during heating.<sup>28,29</sup> The  $12 \times 12 \text{ mm}^2$  format is small relative to that of other CSAF deposition tools.<sup>26,27</sup> However, provided that the spatial resolution of methods used to study the CSAF allow sufficient composition resolution, smaller is better. This allows easier handling of CSAF samples during analysis, and it allows the compact design of the RSM-CSAF deposition tool.

Electron beam sources have been chosen because they allow deposition of elements from a very large part of the periodic table. We have chosen to use commercially available Mantis Deposition Ltd. mini e-beam sources specially fitted with large (5 mm) apertures that give flat source profiles. In principle, different types of physical vapor deposition sources could also be used, provided that they are mounted on 70 mm CFs. The sources are mounted on bellows that allow a small degree of tilt for alignment purposes. A laser mounted on the 70 mm source is used to align the source flanges with the center of the substrate.

The fluxes from the four sources must be calibrated to give roughly equal fluxes at the center of the substrate and then held constant during the deposition process. The UHV chamber houses a Maxtek quartz crystal microbalance (QCM) mounted on an  $xyz$  manipulator that allows the QCM to be positioned at the substrate position for flux measurement during source calibration or moved out of the way during CSAF deposition. The QCM is used to calibrate the deposition rate of each component independently. The QCM also allows calibration of the ion flux monitors that are integral to the e-beam sources. The power to each source can be controlled using the signal from the ion flux monitor to keep the source flux constant during deposition.

The CSAF substrate is mounted on a manipulator that allows it to be positioned accurately and reproducibly in front of the CSAF deposition tool. The position of the substrate holder during deposition is fixed exactly with respect to the RSM-CSAF deposition tool by three positioning pins on the sample stage that is fixed directly to the deposition tool (Fig. 5). The three pins fit into three holes in the substrate mounting mechanism on the substrate manipulator. The substrate manipulator has power feedthroughs to allow heating of the substrate prior to or during CSAF deposition. Finally, the manipulator is designed to allow transfer of the substrate holder to the CSAF analysis systems (ThermoFisher ThetaProbe<sup>TM</sup> and a Tescan Vega3 SEM) with which the CSAF deposition chamber will be integrated.

The RSM-CSAF deposition tool is mounted in a small UHV chamber that can be evacuated to pressures  $<10^{-9}$  Torr using a 500 l/s turbomolecular pump. The RSM-CSAF deposition tool must be mounted at the bottom of the chamber if the sources are going to contain liquid metals during operation. For use with sputter sources, the RSM-CSAF tool could be mounted in any orientation. In addition to the tools mentioned above, the UHV chamber is equipped with an ionization pressure gauge, a leak valve to allow controlled introduction of gases, an  $\text{Ar}^+$  ion gun for sputter cleaning of

the Mo deposition substrate, and a residual gas analyzer for analysis of background gases and detection of leaks.

## B. Performance of the RSM-CSAF deposition tool

Two critical metrics for deposition of CSAFs are the rates of deposition of the various components and the ability to control the composition distribution. The deposition rate must be sufficiently high that it allows the deposition of CSAFs with requisite thickness in a reasonable period of time (1–10 h). In principle, a CSAF thickness of a few nanometers could be sufficient for applications in which the surface properties are important, while thicknesses on the order of a few microns might be necessary, if the property of interest is dominated by bulk materials characteristics. We also find that dewetting can be a critical issue, if thin CSAFs are annealed to high temperatures. Dewetting of the CSAFs renders them useless for many investigations but can be avoided by attention to the nature of the substrate material, the maximum annealing temperature, the CSAF thickness, and the annealing time.

The commercial mini e-beam evaporators used in the RSM-CSAF deposition tool can deposit some metals at rates as high as 1 monolayer per second at the source–substrate working distance of 135 mm, allowing the deposition of a  $1 \mu\text{m}$  thick CSAF in the space of  $\sim 100$  min. More commonly, we use much slower deposition rates of  $\sim 0.02$  monolayer per second from each source, which allows deposition of films that are  $\sim 100$  nm thick in the space of a few hours. To demonstrate the capabilities of the RSM-CSAF deposition tool, we have deposited several  $\text{Cu}_x\text{Au}_y\text{Pd}_{1-x-y}$  CSAFs. Cu, Au, and Pd pellets with 3 mm diameter and 99.99% purity were purchased from the Kurt J. Lesker Company and placed in the molybdenum crucibles of three of the four e-beam evaporation sources. The sources were then aligned and the flux versus power curves were calibrated independently, before depositing the  $\text{Cu}_x\text{Au}_y\text{Pd}_{1-x-y}$  CSAF.

Control of the CSAF composition across the substrate requires some care. The shadow mask technique has the benefit that the deposition flux across the substrate is linear in position, as should be clear from Figs. 2(d), 7, and 8. One merely has to align each source and its mask such that the midpoints of the gradients from all four sources fall along the necessary lines near the center of the substrate. Each of the four 70 mm source flanges has a bellows that allows a small degree of tilt for source alignment. A laser alignment tool was used to align the source flanges. The laser beam is normal to the 70 mm CF and colinear with its center line. The laser beams from all four source flanges must fall on the appropriate points on the substrate to yield the desired composition spread. Furthermore, the shadow mask should always intersect half of the beam at all shadow mask orientations. Fortunately, the design of the RSM-CSAF deposition tool is tolerant of minor misalignments because these simply shift the spatial extents of the composition spreads from each of the four sources. Provided that the maximum and minimum edges of the flux spread from each source lie on the substrate, the full ternary CSAF will be deposited on the

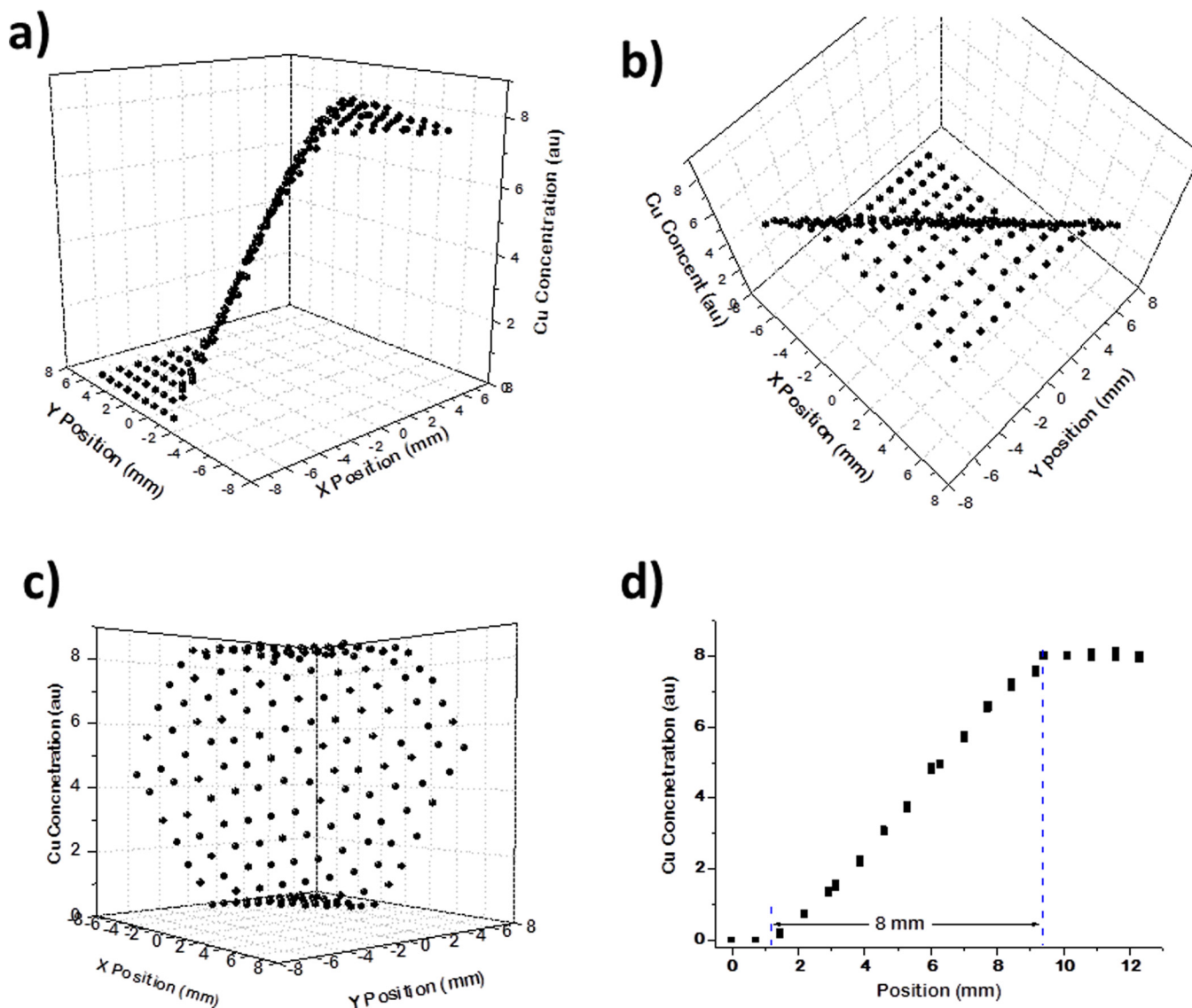


Fig. 7. (Color online) (a)–(c) Different views of the Cu composition profile measured using EDX from a single component Cu film deposited with the rotatable shadow mask in a fixed direction. (d) Cross section of the Cu composition profile along the gradient direction.

face of the  $12 \times 12 \text{ mm}^2$  substrate. The spatial extents of the gradients from the sources are measured to be  $\sim 8 \text{ mm}$  [Fig. 7(d)], which means that the triangular ternary alloy region (Fig. 1) has edges of  $\sim 9 \text{ mm}$  and falls well within bounds of the substrate.

The alignment of the e-beam sources was checked using a QCM that can be positioned at the substrate deposition position. The individual component deposition rates were calibrated by depositing single component films and using both EDX analysis (*ex situ*) and the QCM (*in situ*) to determine the film thickness. Source operating conditions were found that delivered fluxes that were sufficient for CSAF deposition and were high enough to be measured using the ion flux monitors on each of the sources. The current measured by the ion flux monitor was then used to control the source power to deliver constant flux. In tandem, these methods allow calibration of the single component deposition rates to an accuracy of  $< 5\%$ . The Cu, Au, and Pd film composition

distributions across the CSAF were determined using EDX analysis to verify the alignment of the sources, the rotatable shadow masks and the substrate.

In the example presented in Fig. 7, we have deposited a single component, Cu CSAF onto the surface of a polished  $12 \times 12 \text{ mm}^2$  Mo substrate. The Cu source was outgassed before deposition to obtain flux readings arising solely from metal evaporation and not from materials outgassed by the source. As expected, the composition spread has a linear gradient along the direction determined by the orientation of the shadow mask and is constant in the orthogonal direction. There is a constant Cu concentration on one side of the gradient and no detectable Cu on the other side. Clearly, if the shadow mask is held in a fixed orientation during deposition, the composition spread varies linearly between 0 and 100% across the substrate, where 100% indicates the thickness or composition at points that are not shadowed at all from the source and receive its full flux. With the actual source–

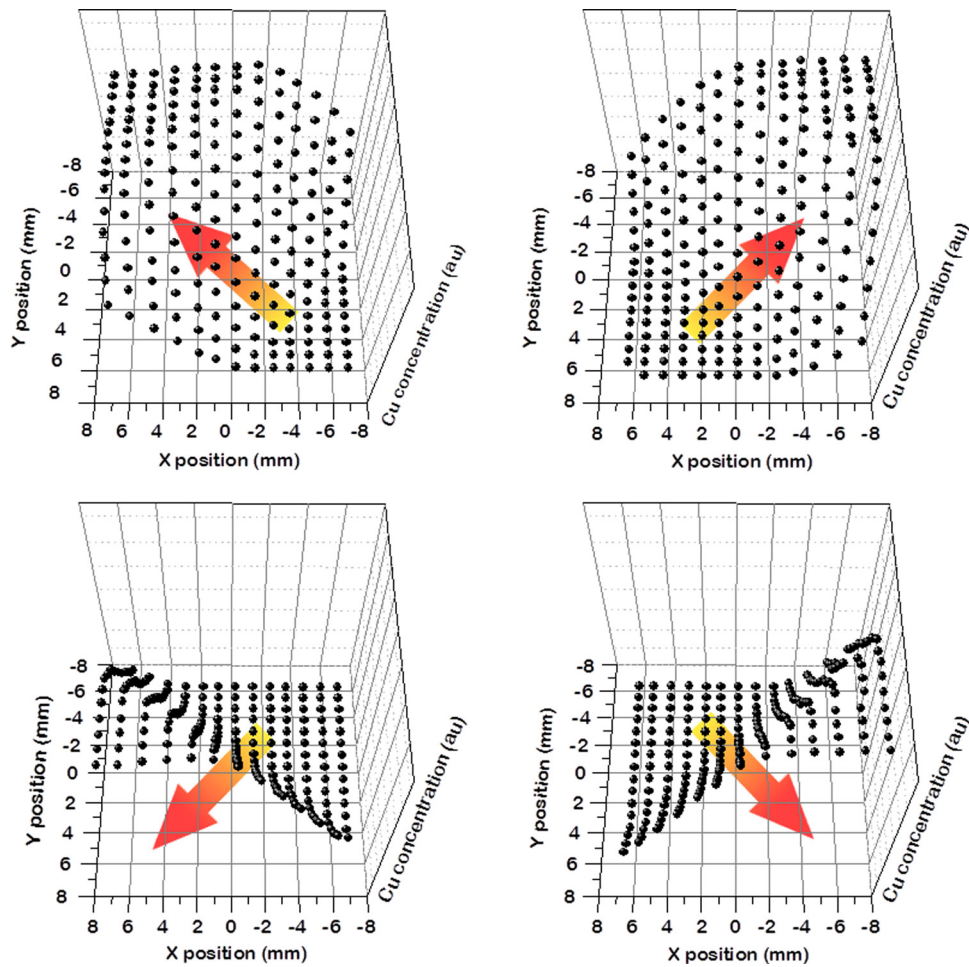


Fig. 8. (Color online) Cu composition maps for four Cu films deposited with the shadow mask in four different positions such that the resulting gradients are rotated by  $90^\circ$  from one another.

mask–substrate spacing, the spatial extent of the gradient is 8 mm [Fig. 7(d)] and it is centered on the substrate.

One of the key features of the RSM-CSAF deposition tool is that rotation of the shadow mask during deposition can be used to control the amplitude of the composition gradient. If the mask spends 75% of the time in one orientation ( $0^\circ$ ) and 25% in the opposite orientation (rotated by  $180^\circ$ ), the CSAF should have the same spatial extent, but its amplitude would go from 25% to 75% of the full source flux. The shadow mask can be rotated through  $180^\circ$  in under 2 s, and so, for a deposition rate corresponding to 1 monolayer in 50 s, there is ample time to hold the shadow mask in one position ( $0^\circ$ ), rotate it, and then hold it in the opposite position ( $180^\circ$ ) during deposition of a single monolayer. Films with composition gradients spanning any desired interval in the range of 0–100% of full flux would be deposited by cycling the mask position once per monolayer, thus achieving codeposition of the components and intimate intermixing without annealing. In the previously described deposition of CSAFs using a fixed shadow mask,<sup>26,27</sup> a similar partial gradient is achieved by varying the position of the shadow and the net source flux. Our implementation requires only rotation of the shadow mask while holding the source flux constant. As a simple initial demonstration of this capability, a

Cu film has been grown while rotating the shadow mask at a constant rate of  $12^\circ/\text{s}$ . The EDX maps in Fig. 9 show that there is no net gradient in Cu concentration across the substrate. We do observe a small decrease in Cu concentration in the middle of the substrate, which we attribute to a minor misalignment of the semicircular shadow mask. Moreover, we observe a slight gradient in film composition in the direction of source inclination [Fig. 9(b)]. As described previously, the deposition tubes are tilted by an angle of  $15^\circ$  with respect to the center line of the flange on which the RSM-CSAF deposition tool is mounted. The flux at the substrate surface depends on the distances between points on the substrate and points across the source surface, thus causing a slight composition gradient in the tilt direction.

Creating a linear gradient in the alloy composition (elemental component fractions) is more difficult than simply having a linear gradient in the component fluxes because it requires that the deposition rates of the components be identical. For example, consider the deposition of a binary CSAF,  $A_xB_{1-x}$ , where the two components are deposited from opposing directions. The distribution of A across the substrate is given by  $A(\xi) = \xi * A_0$  and the distribution of B is  $B(\xi) = (1 - \xi) * B_0$ , where  $A_0$  and  $B_0$  are the maximum amounts of the two components deposited at either end of the

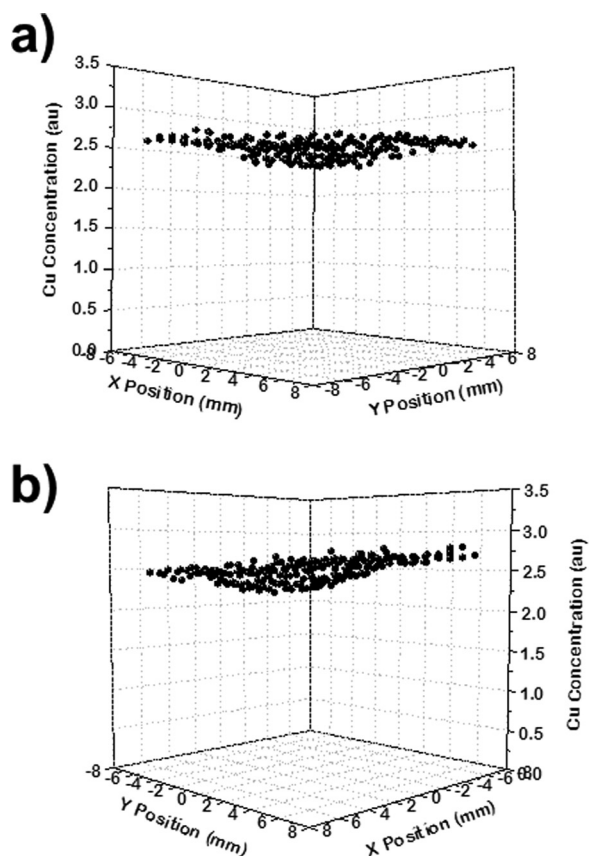


FIG. 9. (a) Cu composition profile measured using EDX analysis of a single component Cu film deposited with continuous rotation of the shadow mask during the deposition. Rotation of the mask results in deposition of a fairly uniform film. (b) Cu composition profile along the source inclination direction. The inclination of the source with respect to the substrate does generate a slight flux gradient.

substrate, and  $\xi$  is the position on the substrate. Although the flux of each component is linear in the position, the fraction of A forming the alloy at a given position on the surfaces is given by  $x(\xi) = \xi * A_0 / (B_0 + \xi * (A_0 - B_0))$ . When  $A_0 = B_0$ , the gradient in the component fraction across the substrate is linear in position. However, the composition is clearly non-linear in position if  $A_0 \neq B_0$ . For ternary CSAFs generated by having three components deposited with fluxes at  $120^\circ$  from one another, the component fluxes at the three corners (Fig. 1) must be identical to give a CSAF with a linear gradient in composition such that the positions on the CSAF map directly onto a ternary composition diagram.

Finally, we tested the RSM-CSAF deposition tool by making a  $\text{Cu}_x\text{Pd}_y\text{Au}_{1-x-y}$  ternary CSAF with the shadow masks oriented at  $120^\circ$  from one another. With these source settings, the deposition rates of all three metals were 2.2 nm/min and all three were codeposited for 45 min to generate a 100 nm thick CSAF. The RSM-CSAF deposition tool works as designed. As illustrated in Fig. 10, the distribution of each component has a linear gradient along the expected direction with equal maximum amounts at the three corners of the CSAF. With the EDX analyses, we have measured the local composition of the CSAF on a square grid with 1 mm spacing, and we have plotted the compositions at these points on the ternary composition diagram shown in Fig. 10(d). It is

immediately obvious that, in contrast to the composition spread prepared with the offset filament tool (Fig. 3), the ternary CSAF generated by with RSM-CSAF deposition tool spans the entire ternary composition space. The fairly uniform spacing of points across the ternary composition diagram indicates that the fluxes from each of the three sources are roughly equal. The high density of points along the edges (pure binaries) arises from the fact that, as illustrated in Fig. 1, there are regions of the CSAF where the flux from one source is zero and thus, only two components are deposited. Finally, in Fig. 1, we have already provided a photograph of the  $\text{Cu}_x\text{Pd}_y\text{Au}_{1-x-y}$  as deposited on the Mo substrate. The Au, Cu, and Pd regions are evident by the differences in their color.

### C. Assessment of the RSM-CSAF deposition tool

The RSM-CSAF deposition tool described in this work has a number of advantages over the methods illustrated in Fig. 2. Principally, in one CSAF, we can prepare all possible compositions of a ternary system: the pure components A, B, and C; all possible binaries  $A_xB_{1-x}$ ,  $A_xC_{1-x}$ , and  $B_xC_{1-x}$  (with  $x = 0-1$ ); and in the center of the CSAF, all possible compositions of a ternary alloy  $A_xB_yC_{1-x-y}$  ( $x = 0 \rightarrow 1$ ,  $y = 0 \rightarrow 1-x$ ) (Figs. 1 and 10). It is more compact than previous implementations of the shadow mask method<sup>26,27</sup> in that the entire deposition tool with all four sources is integrated onto one 254 mm CF flange for mounting onto a standard UHV chamber. Rather than using linear motions of the shadow masks and keeping them fixed during deposition, we have chosen to incorporate rotation of the masks during deposition for controlling the range and the direction of the gradients from each of the sources. By rotating the masks during deposition, the composition gradient can be controlled to give uniform composition, a composition varying from 0 to 100% across the CSAF, or any range in between. The CSAF deposition tool coupled with the ability to perform spatially resolved analysis will allow comprehensive study of a number of surface science and materials science problems that are otherwise intractable. The RSM-CSAF deposition tool will be attached to a SEM/EDX/EBSD analysis apparatus that will allow ready determination of phase diagrams across composition space.<sup>25</sup> An identical sister tool will be attached to an apparatus for spatially resolved XPS/UPS/LEIS, to enable high throughput study of alloy surface phenomena such as segregation.<sup>25,30</sup> Finally, when coupled to a  $10 \times 10$  multichannel microreactor array, these CSAFs will enable rapid study of alloy catalysis across composition space. In general, well characterized CSAFs of the type described can be used to accelerate the study of number bulk and surface phenomena.

Nevertheless, there are limitations and issues associated with the study of CSAFs that must be addressed. A thin film is not a bulk material. Its bulk and surface properties can be influenced by the substrate and by the deposition method. In most cases, such thin films will not be single crystals, unless grown epitaxially on a single crystalline substrate, and even so such a film must be under stress because its lattice constant will not match that of the substrate perfectly. For an application or problem of interest, all such issues can be

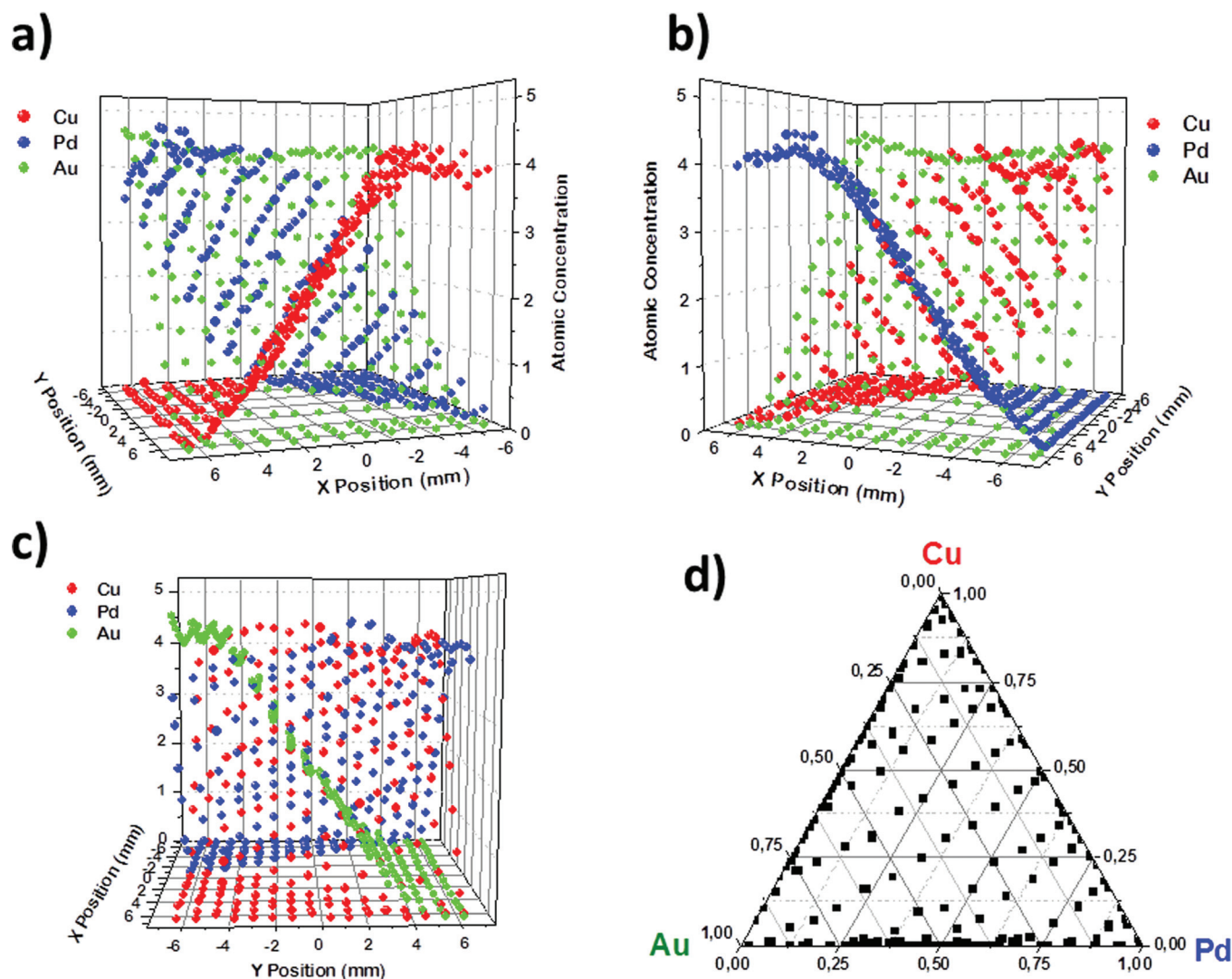


FIG. 10. (Color) (a)–(c) Compositions measured by EDX of a  $\text{Cu}_x\text{Pd}_y\text{Au}_{1-x-y}$  CSAF deposited with the rotatable shadow masks oriented at  $120^\circ$  from one another. The three plots show the composition of the same film viewed from different orientations. (d) The distribution of CSAF compositions across a ternary composition diagram, indicating complete and fairly uniform coverage of ternary composition space. Points are distributed on a  $1\text{ mm} \times 1\text{ mm}$  spatial grid across the CSAF. The high density of points along the perimeters reflects the fact that the CSAF contains regions that are binary alloys.

addressed by the use of appropriate control studies using different substrates, growing films of different thickness, and using various deposition conditions. It should be noted that by using the rotatable shadow mask properly one can grow thin binary alloy films with composition variation in one direction and thickness variation in the orthogonal. Thus, the impact of film thickness on a given alloy property can be studied in a high throughput manner. It should be pointed out that the limitations mentioned here are not specific to the use of CSAFs but apply to all thin film science. In spite of these limitations, the use of CSAFs has the potential to rapidly advance progress in many important areas of surface science and materials science.

### III. CONCLUSION

A compact tool for deposition of CSAFs has been developed and demonstrated. The individual component deposi-

tion rates were calibrated using EDX analysis, single component films, and a QCM. Films of pure Cu and  $\text{Cu}_x\text{Pd}_y\text{Au}_{1-x-y}$  CSAFs were prepared to demonstrate the performance of the deposition tool. Experimental measurements of compositions across the CSAF match expectations. The orientation of the mask can be used to control the amplitude and orientation of the composition gradient across the substrate. By rotating the mask during deposition, the composition gradient can be controlled to give uniform composition, a composition varying from 0 to 100% across the sample, or any range in between. With this UHV RSM-CSAF deposition tool, we can prepare a multicomponent material with lateral composition gradients of each element deposited in any direction to reproduce directly all compositions of a ternary composition diagram. CSAF libraries prepared using this deposition tool will enable rapid determination of composition–structure–property relationships across continuous regions of alloy composition space.

## ACKNOWLEDGMENTS

Transfer Engineering and Manufacturing, Inc. (Fremont, CA) fabricated the RSM-CSAF deposition tool. Support is acknowledged from the NSF under Grant No. CBET-0923083. As part of the National Energy Technology Laboratory's Regional University Alliance (NETL-RUA), a collaborative initiative of the NETL, this technical effort was performed under the RES Contract No. DE-FE0004000. This project was funded, in part, by the Department of Energy, National Energy Technology Laboratory, an agency of the United States Government, through a support contract with URS Energy & Construction, Inc. Neither the United States Government nor any agency thereof, nor any of their employees, nor URS Energy & Construction, Inc., nor any of their employees, makes any warranty, expressed or implied, or assumes any legal liability or responsibility for the accuracy, completeness, or usefulness of any information, apparatus, product, or process disclosed, or represents that its use would not infringe privately owned rights. Reference herein to any specific commercial product, process, or service by trade name, trademark, manufacturer, or otherwise does not necessarily constitute or imply its endorsement, recommendation, or favoring by the United States Government or any agency thereof. The views and opinions of authors expressed herein do not necessarily state or reflect those of the United States Government or any agency thereof.

<sup>1</sup>I. Takeuchi, R. B. van Dover, and H. Koinuma, *MRS Bull.* **27**, 301 (2002).

<sup>2</sup>S. I. Woo and S. H. Kim, *Top. Catal.* **53**, 1 (2010).

<sup>3</sup>J. C. Hogan, *Nat. Biotechnol.* **15**, 328 (1997).

<sup>4</sup>J. P. Kennedy, L. Williams, T. M. Bridges, R. N. Daniels, D. Weaver, and C. W. Lindsley, *J. Comb. Chem.* **10**, 345 (2008).

<sup>5</sup>J. Cui *et al.*, *Nat. Mat.* **5**, 286 (2006).

<sup>6</sup>J. Wang and K. E. Gonsalves, *J. Comb. Chem.* **1**, 216 (1999).

<sup>7</sup>J. N. Cawse, D. Olson, B. J. Chisholm, M. Brennan, T. Sun, W. Flanagan, J. Akhave, A. Mehrabi, and D. Saunders, *Prog. Org. Coat.* **47**, 128 (2003).

<sup>8</sup>K. W. Kim, M. K. Jeon, K. S. Oh, T. S. Kim, Y. S. Kim, and S. I. Woo, *Proc. Nat. Acad. Sci. U.S.A.* **104**, 1134 (2007).

<sup>9</sup>X. D. Xiang, X. Sun, G. Bricena, Y. Lou, K. A. Wang, H. Chang, W. G. Wallace-Freedman, S. W. Chen, and P. G. Schultz, *Science* **268**, 1738 (1995).

<sup>10</sup>J. S. Cooper and P. J. McGinn, *Appl. Surf. Sci.* **254**, 662 (2007).

<sup>11</sup>N. C. Woo, B. G. Ng, and R. B. V. Dover, *Rev. Sci. Instrum.* **78**, 072208 (2007).

<sup>12</sup>O. L. Warren and T. J. Wyrobek, *Meas. Sci. Technol.* **16**, 100 (2005).

<sup>13</sup>K. Kennedy, T. Stefansky, G. Davy, V. F. Zackay, and E. R. Parker, *J. Appl. Phys.* **36**, 3808 (1965).

<sup>14</sup>J. J. Hanak, *J. Mater. Sci.* **5**, 964 (1970).

<sup>15</sup>A. Boettcher, G. Haase, and R. Thun, *Zeitschrift Fur Metallkunde* **46**, 386 (1955).

<sup>16</sup>J. S. Wang, Y. Yoo, C. Gao, I. Takeuchi, X. D. Sun, H. Y. Chang, X. D. Xiang, and P. G. Schultz, *Science* **279**, 1712 (1998).

<sup>17</sup>S. E. Russek, W. E. Bailey, G. Alers, and D. L. Abraham, *IEEE Trans. Magn.* **37**, 2156 (2001).

<sup>18</sup>S. E. Russek, P. Kabos, R. D. McMichael, C. G. Lee, W. E. Bailey, R. Ewasko, and S. C. Sanders, *J. Appl. Phys.* **91**, 8659 (2002).

<sup>19</sup>Q. Wang, F. Liu, and D. Han, *Macromol. Rapid Commun.* **25**, 326 (2004).

<sup>20</sup>Q. Wang, Y. Guozhen, J. Li, and D. Han, *Solid State Commun.* **113**, 175 (2000).

<sup>21</sup>I. Ohkubo, H. M. Christen, P. Khalifah, S. Sathyamurthy, H. Y. Zhai, C. M. Rouleau, D. G. Mandrus, and D. H. Lowndes, *Appl. Surf. Sci.* **223**, 35 (2004).

<sup>22</sup>Y. Yamada, T. Fukumura, M. Ikeda, M. Ohtani, H. Toyosaki, A. Ohtomo, F. Matsukura, H. Ohno, and M. Kawasaki, *J. Supercond.* **18**, 109 (2005).

<sup>23</sup>M. Bate, C. Neuber, R. Giesa, and H.-W. Schmidt, *Macromol. Rapid Commun.* **25**, 371 (2004).

<sup>24</sup>R. B. van Dover and L. F. Schneemeyer, *Macromol. Rapid Commun.* **25**, 150 (2004).

<sup>25</sup>D. Priyadarshini, P. Kondratyuk, J. B. Miller, and A. J. Gellman, *J. Vac. Sci. Technol. A* **30**, 011503 (2012).

<sup>26</sup>S. Guerin and B. E. Hayden, U.S. patent 0,275,164 (29 Nov. 2007).

<sup>27</sup>S. Guerin and B. E. Hayden, *J. Comb. Chem.* **8**, 66 (2006).

<sup>28</sup>C. Park, E. Bauer, and H. Poppa, *Surf. Sci.* **154**, 371 (1985).

<sup>29</sup>J. W. He, W. L. Shea, X. Xiang, and D. W. Goodman, *J. Vac. Sci. Technol. A* **8**, 2435 (1990).

<sup>30</sup>J. B. Miller, D. Priyadarshini, and A. J. Gellman, *Surf. Sci.* **606**, 1520 (2012).